Kinetics alteration of the $6Mg(NH_2)_2$-$9LiH$-$LiBH_4$ system by co-adding YCl_3 and Li_3N

Hujun Cao,[a] Weijin Zhang,[b] Claudio Pistidda,[a] Júlian. Puszkiel,[a] Chiara Milanese,[c] Antonio Santoru,[a] Fahim Karimi,[a] Maria Victoria Castro Riglos,[a] Gökhan Gizer,[a] Edmund Welter,[d] Jozef Bednarcik,[d] Martin Etter,[d] Ping Chen,[b] Thomas Klassen[a] and Martin Dornheim[a]*

a. Institute of Materials Research, Materials Technology, Helmholtz-Zentrum Geesthacht GmbH, Max-Planck-Straße 1, D-21502, Geesthacht, Germany.

E-Mail: hujun.cao@hzg.de; Fax: + 49 04152 / 87-2625; Tel: +49 04152 / 87-2643

b. Dalian National Laboratory for Clean Energy Dalian Institute of Chemical Physics, Chinese Academy of Sciences, Dalian 116023, China.

c. Pavia H2 Lab, Department of Chemistry, Physical Chemistry Section, University of Pavia, VialeTaramelli 16, I-27100 Pavia, Italy.

d. Deutsches Elektronen-Synchrotron a Research Centre of the Helmholtz Association, Notkestraße 85, Germany.

Abstract:

The $6Mg(NH_2)_2$-$9LiH$-$LiBH_4$ system has a reversible hydrogen content of ~ 4.2 wt.% and a calculated equilibrium pressure of 1 bar hydrogen at ~ 64 °C.[1] However, the existence of severe kinetic barriers inhibits the de/re-hydrogenation processes to occurr at such low temperature. In this work, Li_3N and YCl_3 have been chosen as co-additives for the $6Mg(NH_2)_2$-$9LiH$-$LiBH_4$ system. These additives increase the hydrogen storage capacity of the system and hasten the de/re-hydrogenation kinetics: the total capacity of 4.2 wt. % of H_2 was achieved in only 8 min under isothermal conditions at 180 °C and 85 bar of H_2 pressure. The re-hydrogenation temperature, necessary for a complete absorption process, can be lowered below 90 °C by increasing the H_2 pressure above 185 bar. Moreover, the results indicate that the hydrogenation capacity and absorption kinetics can be maintained roughly constant over several cycles. The low operating temperatures with fast absorption kinetics and good reversibility make this system a promising candidate for on-board hydrogen storage material. The reasons for the improved hydrogenation/dehydrogenation properties are thoroughly investigated and discussed.

Introduction

With the ever-increasing consumption of fossil fuels and along with the associated environmental problems, it urges to develop technologies enabling us to effectively exploit renewable energy sources. In order to achieve such a goal, it is of primary importance to find efficient and ecofriendly energy carriers.[2] Hydrogen is one of the promising alternatives to conventional fossil fuels due to its high energy density and environmental compatibility.[3] Owning to their high hydrogen contents, in the past decades, light element complex hydrides such as alanates,[4] borohydrides[5] and amide-hydride composite systems[6, 7] have been investigated as potential hydrogen storage materials.[8] Since 2002,[6] amide-hydride composite

systems are extensively investigated because of their suitable thermodynamic stability, good reversibility and high hydrogen content. In particular, Li-Mg-N-H ($Mg(NH_2)_2$-xLiH, x=2, 8/3, 4) composite system was developed in 2004. [9, 10] Among the studied amide-hydride ratios, $Mg(NH_2)_2$-2LiH[10] attracted high attention due to its appealing features, i.e. gravimetric hydrogen capacity (ca. 5.6 wt.%), dehydrogenation enthalpy (ΔH ca. 40 kJ/mol_{H2}), high equilibrium pressure and excellent reversibility. Based on the thermodynamic data, the expected dehydrogenation temperature is about 90 °C at 1 bar of H_2 pressure. Noticeably, this temperature falls within the operating temperature range of proton exchange membrane fuel cells (PEMFCs).[11] However, for practical applications, suitable dehydrogenation rates can only be obtained at temperatures above 180 °C as a result of severe kinetic barriers ($Ea \approx 130$ kJ mol^{-1}).[12] This high activation energy was inferred to the sluggish interface reaction between amide and hydride in the preliminary reaction stage and to the hindered mass transport through the as-formed imide layer in the following step.[13] Many strategies have been developed to overcome the kinetic barriers and to reduce the reaction enthalpy of the Li-Mg-N-H system.[14, 15] Compared with the pristine Li-Mg-N-H system, potassium/rubidium compounds, such as KH, RbH, KOH, KF, RbOH,[14] are observed to lower the desorption temperature by ca. 50 °C. The addition of metals/metal salts (Si, Al, $TiCl_3$, VCl_3, $ScCl_3$ and $NiCl_2$ etc.) and metal nitrides (Li_3N, TaN and TiN) to this system can effectively improve the sorption kinetics of the Li-Mg-N-H system.[16] Borohydrides play an important role in improving the hydrogen storage properties of the Li-Mg-N-H system.[1, 17, 18, 19] For example, in comparison to $LiNH_2$-MgH_2, $LiNH_2$-$LiBH_4$ and MgH_2-$LiBH_4$ the $LiNH_2$-MgH_2-$LiBH_4$ mixture shows enhanced hydrogen storage properties.[17] Hu et al.[19], intensively, investigated the effect of $LiBH_4$ on the $Mg(NH_2)_2$-2LiH system, and found that $LiBH_4$ not only improves the kinetic property but also reduces the

thermodynamic stability. For instance, the $Mg(NH_2)_2$-2LiH-0.1$LiBH_4$ system can release 5 wt.% of H_2 at 140 °C and be fully re-hydrogenated at 100 °C and 20 h. The addition of $LiBH_4$, reduces the dehydrogenation enthalpy (ΔH) from 40 to 36.5 kJ $(mol\text{-}H_2)^{-1}$. By varying the molar ratio of $Mg(NH_2)_2$, LiH and $LiBH_4$, it was found that the optimum $Mg(NH_2)_2$:LiH:$LiBH_4$ molar ratio is 6:9:1. After stabilizing the dehydrogenated state through the formation of $Li_4BN_3H_{10}$ (reaction 1), an equilibrium pressure of 1 bar of hydrogen is thermodynamically allowed at ca. 64 °C.[1] However, no de/re-hydrogenation is observed at temperatures below 100 °C under vacuum and 80 bar of H_2, respectively.

$$6Mg(NH_2)_2 + 9LiH + LiBH_4 \leftrightarrow 3Li_2Mg_2(NH)_3 + Li_4BN_3H_{10} + 9H_2 \quad (1)$$

Considering that transition metal salts and nitrides independently show positive effects on the de/re-hydrogenation reaction kinetics of the Li-Mg-N-H systems, in this work, YCl_3 and Li_3N are used together as co-additives in the 6$Mg(NH_2)_2$-9LiH-$LiBH_4$. The hydrogen storage properties and the reaction mechanisms of this co-doped are investigated by volumetric methods, differential thermal analyses (DTA), temperature programmed mass spectrometry (TPD-MS) *in situ* synchrotron radiation powder X-ray radiation diffraction (SR-PXD), Fourier transform infrared spectroscopy (FT-IR), extended X-ray absorption fine-structure spectroscopy (EXAFS) and high resolution transmission electron microscopy (HR-TEM).

Results and discussion

Dehydrogenation properties

The DTA traces measured for 6$Mg(NH_2)_2$-9LiH-$LiBH_4$ doped with different amounts of YCl_3 and Li_3N were summarized, respectively, in **Figure 1**. For the YCl_3-doped samples, the endothermic peak related to the release of gaseous hydrogen shifts slightly to lower temperatures ($\Delta T \approx 8$ °C). The onset temperature appears to be independent from the amount of YCl_3 contained

in the samples. However, an exothermic peak appears at *ca*. 140 °C is observed in the sample with 10 wt.% of YCl_3. This phenomenon may be connected to the formation of a solid solution between LiCl and $LiBH_4$[20] (LiCl is formed during ball milling, **Figure S1**). Based on these experiments, the content of YCl_3 is fixed at 2 wt.%. In fact, this amount of YCl_3 allows having a low desorption temperature without sacrificing much of the total hydrogen capacity (0.08wt. %). Compared to the pristine system, in the Li_3N-doped system the main endothermic signal is split in two partially overlapping peaks: one shifts to lower temperature, and the other one shifts to higher temperature (Figure 1(b)). This shows that Li_3N can clearly alter the reaction pathway of the composite system $6Mg(NH_2)_2$-9LiH-$LiBH_4$. Among the tested compositions, the DTA trace of the 5wt.% Li_3N-doped sample has the lowest onset temperature. Usually, at temperatures above 140 °C and under H_2 pressure, Li_3N is prone to convert into $LiNH_2$ and LiH. Therefore, it's reasonable to expect that the addition of Li_3N could positively affect the overall hydrogen capacity and change the ratios of amide and hydride phases in this system. For this reason, the amount of Li_3N has been fixed to 5 wt.%.

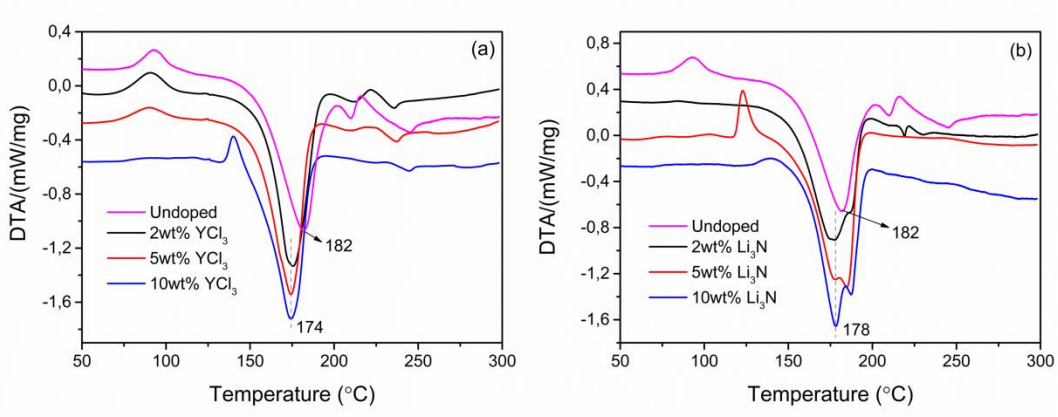

Figure 1. DTA traces of $6Mg(NH_2)_2$-9LiH-$LiBH_4$-xYCl_3 (x=0, 2, 5, 10 wt.%) (a), and $6Mg(NH_2)_2$-9LiH-$LiBH_4$-xLi_3N (x=0, 2, 5, 10 wt.%); (b) The samples were heated from 30 to 300 °C with a heating rate of 3 °C min^{-1}, under 50 mL min^{-1} of argon flow.

The use of combined temperature-programmed dehydrogenation and mass spectrometry (TPD-MS) (**Figure 2**) reveals that the dehydrogenation peaks of all the doped samples are shifted to lower temperatures, in good agreement with the DTA results (Figure 1). Traces of ammonia can be detected at temperatures higher than 190 °C in the undoped and 2wt.% YCl_3-doped samples. The signal of ammonia is almost undetectable in the Li_3N-containing samples, which proves that Li_3N hinders the release of ammonia. All the investigated material appears not to release diborane during the heat treatment.

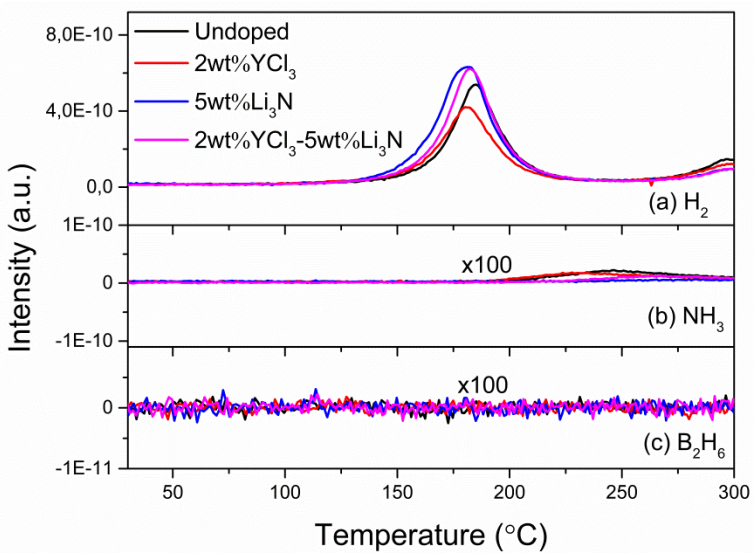

Figure 2. TPD-MS curves of (a) H_2, (b) NH_3 and (c) B_2H_6 releasing from the $6Mg(NH_2)_2$-9LiH-$LiBH_4$ samples without of additives (undoped), doped with 2wt.% YCl_3, doped with 5wt.% Li_3N and co-doped with 5wt.% Li_3N and 2wt.% YCl_3. The samples were heated from 30 to 300 °C with a heating rate of 3 °C min^{-1}, under 50 mL min^{-1} of argon flow.

To investigate the effects of YCl_3 and Li_3N in the $6Mg(NH_2)_2$-9LiH-$LiBH_4$ composite system, the isothermal dehydrogenation of the 2wt.% YCl_3-doped, 5wt.% Li_3N-doped, 2wt.% YCl_3-5wt.% Li_3N-co-doped as well as the pristine sample were measured and the results are plotted in **Figure 3(a)**. It can be seen that the desorption kinetics of the doped samples are faster, especially for the co-doped sample, than that of the pristine sample. For all investigated samples the activation energies were determined by Kissinger's method [21], and the results are summarized

in Figure 3(b). The specific rate constant *k* (Table 1) under a fixed temperature is calculated by Arrhenius equation.[22] (Detailed information shown in SEI).

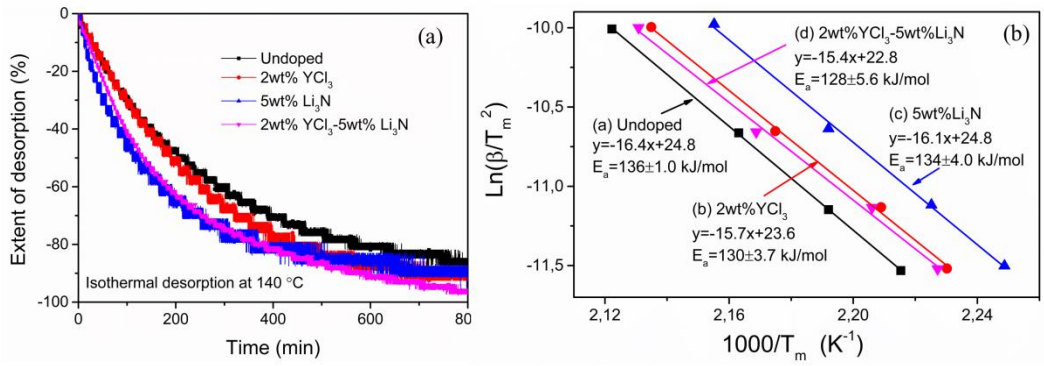

Figure 3. Isothermal dehydrogenation curves at 140 °C and 1 bar of H_2 pressure (a) and activation energies (b) of the undoped, 2wt.% YCl_3, 5wt.% Li_3N and 2wt.% YCl_3-5wt.% Li_3N doped samples,

In comparison with the pristine sample, the activation energies of 2wt. % YCl_3-doped and 5wt. % Li_3N-doped samples are reduced by ca. 6 and 2 kJ mol^{-1}, respectively. The co-doped sample has the lowest E_a ca. 128 kJ mol^{-1}, which is 8 kJ mol^{-1} lower than that of the pristine sample. Interestingly, the decrease of activation energy of the co-doped sample is equal to the sum value from the 2wt.% YCl_3-doped and 5wt.% Li_3N-doped samples, which suggests a synergic effect of YCl_3 and Li_3N. All the specific rate constants of the doped samples are higher than that of the pristine sample at different temperatures, which consists with the isothermal dehydrogenation results (Figure 3(a)).

Table 1. E_a, A and *k* values at 90, 100, 140 and 180 °C, calculated from the Kissinger's and the Arrhenius equations.

Name	E_a (kJ mol^{-1})	*A* (min^{-1})	*K* (90 °C) (min^{-1})	*K* (100 °C) (min^{-1})	*K* (140 °C) (min^{-1})	*K* (180 °C) (min^{-1})
Free	136±1.0	5.7E10	1.4E-9	4.8E-9	3.4E-7	1.1E-5
2wt%YCl_3	130±3.7	1.8E10	2.6E-9	8.4E-9	5.0E-7	1.4E-5
5wt%Li_3N	134±4.0	5.8E10	2.9E-9	9.4E-9	6.2E-7	2.0E-5
5wt%Li_3N-2wt%YCl_3	128±5.6	8.0E9	3.0E-9	9.3E-9	5.1E-7	1.4E-5

Hydrogenation and reversibility properties

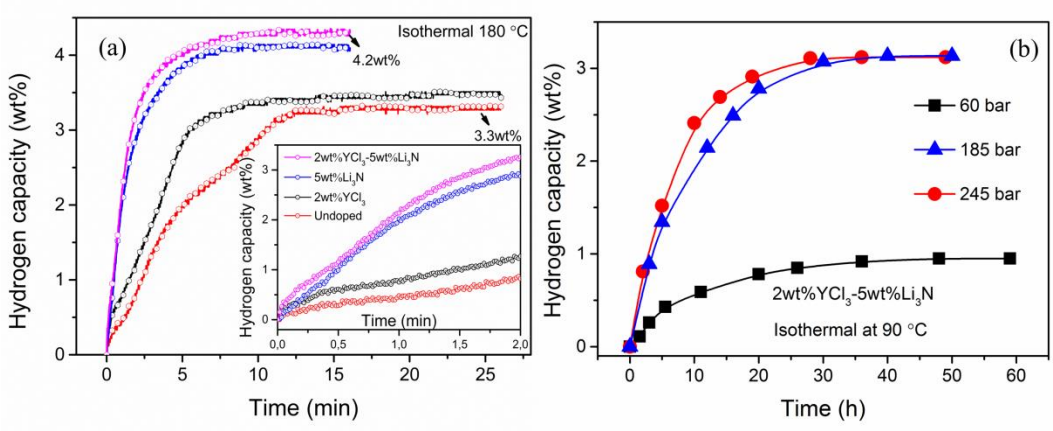

Figure 4. (a) Isothermal hydrogenation curves of the pristine system, 2wt.% YCl_3, 5wt.% Li_3N and 2wt.% YCl_3-5wt.% Li_3N-co-doped samples at 180 °C and 50 bar. Inset is the isothermal hydrogenation curves of these samples at the first 2 min; (b) Isothermal hydrogenation of the 2wt.% YCl_3-5wt.% Li_3N-co-doped sample at 90 °C under 60, 185 and 245 bar of H_2, respectively. (Before hydrogenation, all the samples were fully dehydrogenated isothermally at T=180 °C).

The results of isothermal re-hydrogenation measurements of these samples at 180 and 90 °C are presented in **Figure 4**. Isothermal hydrogenation at 180 °C shows that all the doped samples can be hydrogenated completely within 10 min, especially, the co-doped sample is hydrogenated more than 4 wt.% of hydrogen in the first 5 min and a further ~ 0.2 wt.% in the following 3 min (Figure 4(a)). Both the Li_3N containing samples show a faster absorption rate than the sample doped only with YCl_3, especially at the first stage. It's clearly visible from the inlet in Figure 4(a), that the co-doped sample has the best re-hydrogenation kinetics in the first 2 min. We believe that by further optimizing the composition of the co-doped sample, the target of charging rate fixed from the DOE for on-board applications could be fulfilled.[23] Lowering the temperature to 140 °C, only about 1.1 wt% of H_2 is absorbed by the pristine sample in the first 100 min; however the co-doped sample has been hydrogenated to the maximum hydrogen content of 4.3 wt% of H_2 in 80 min (**Figure S2**). As for the desorption measurements showed, the co-doped samples have the fastest absorption kinetics among all the investigated samples. The YCl_3-containing samples, however, show better kinetics than those of the Li_3N-doped

samples during the time-range from 30 to 60 min. It is likely that Li_3N might influence the first stage of the reaction, whereas YCl_3 possibly influence the later stage. Therefore the improved absorption properties of the co-doped system can be explained considering these two additives play complementary roles. The effect of the applied H_2 pressures (from 60 to 245 bar) on the absorption process performed at 90 °C was investigated for the co-doped sample (Figure 4(b)). The co-doped sample can be fully re-hydrogenated at 90 °C and H_2 pressures above 185 bar in 38 hours. The temperature value of 90 °C already meets the PEMFCs operating conditions.[11] By slightly increasing the temperature from 90 °C to 100 °C, the co-doped sample can be fully re-hydrogenated under only 50 bar of H_2 (**Figure S3**).

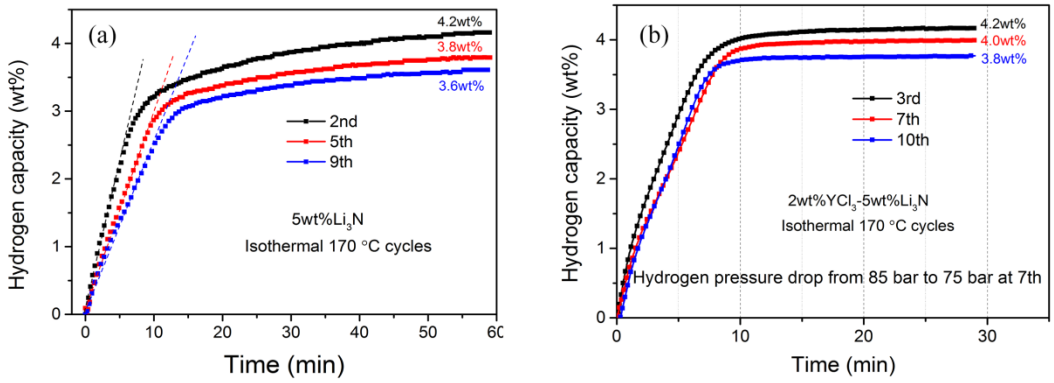

Figure 5. Isothermal hydrogenation curves relative to (a) the 2nd, 5th and 9th cycle of the 5wt. %Li_3N-doped sample; (b) the 3rd, 7th and 10th cycle of the co-doped sample, at 170 °C and 85 bar of H_2. It should be pointed out that the H_2 pressure during the absorption measurements dropped from 85 to 75 bar after the 7th cycles. This could be one of the reasons for the reduced reversible hydrogen capacity.

The reversibility of the 5wt. % Li_3N-doped and co-doped samples were plotted in **Figure 5**. Figure 5(a) shows that the reversible hydrogen content after 9 cycles decreases from 4.2 wt. % to 3.6 wt. % and the re-hydrogenation rate also decreases over cycling. In contrast, the reversible hydrogen capacity of the co-doped sample is higher than that of the Li_3N-doped sample: even after 10 cycles the hydrogen content is more than 3.8 wt. % (Figure 5(b)). From these volumetric

analyses, it appears that the kinetic properties of the co-doped sample are kept almost unchanged over several cycles. Interestingly, all the absorption reactions of the co-doped sample are completed within 10 min even after 10 cycles.

Reaction mechanism

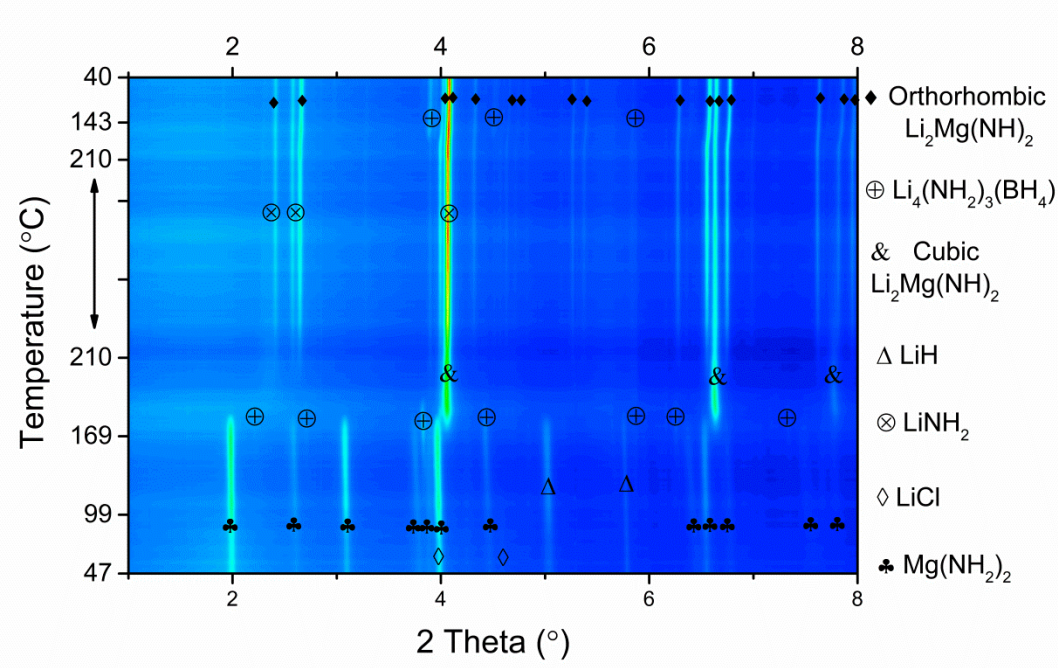

Figure 6. *In situ* SR-PXD dehydrogenation of the co-doped sample. It was heated from room temperature (RT) to 210 °C and kept at 210 °C for 20 min under vacuum. The heating and cooling rates were 10 and 20 °C/min, respectively.

In situ SR-PXD was used to record the dehydrogenation reaction pathway of the co-doped system (**Figure 6**). The starting diffraction patterns indicate the presence of $Mg(NH_2)_2$, LiH and LiCl. LiCl is produced from the metathesis reaction between LiH and YCl_3 (Figure S1). It should be noted that the diffraction peaks of $Mg(NH_2)_2$ could be detected clearly here, differently from the pristine sample. Indeed, in the pristine system, $Mg(NH_2)_2$ under the same mechanochemical process undergoes amorphization (**Figure S4**). Hu et al.,[24] pointed out that the amorphous $Mg(NH_2)_2$ re-crystallizes in the presence of $LiBH_4$ at ca. 150 °C in the $LiBH_4$-doped $Mg(NH_2)_2$-2LiH system, and the N-atom matrix in the crystalline form of $Mg(NH_2)_2$ is one of the key

factors for achieving fast dehydrogenations.[24] Upon heating, $Li_4(NH_2)_3(BH_4)$ forms at around 130 °C and disappears at ca. 180 °C, close to the melting point previously reported (ca. 187 °C).[25] With the sudden disappearance of $Mg(NH_2)_2$, LiH and $Li_4(NH_2)_3(BH_4)$, cubic $Li_2Mg(NH)_2$ is formed at ca. 210 °C and it converts to the orthorhombic polymorph during the isothermal process. After cooling to RT, it is possible to identify the reflections of $Li_2Mg(NH)_2$ and $Li_4(NH_2)_3(BH_4)$. The formation of $Li_4(NH_2)_3(BH_4)$ clearly shows the high reactivity of $LiBH_4$ with Li_3N. We strongly believe that the existence of a single phase (i.e. $Li_4(NH_2)_3(BH_4)$) containing both the amide and the borohydride groups greatly helps the dehydrogenation process by allowing a continuous exchange of amides and borohydrides anions. This might be particularly true when the reaction takes place in the liquid state.[26] In addition, $Li_4(NH_2)_3(BH_4)$ could also offer weaker N-H bonds[27] and accelerate the transport of Li^+ even in solid-state (2×10^{-4} S/cm at RT) [28], given its relatively high lithium conductivity values.

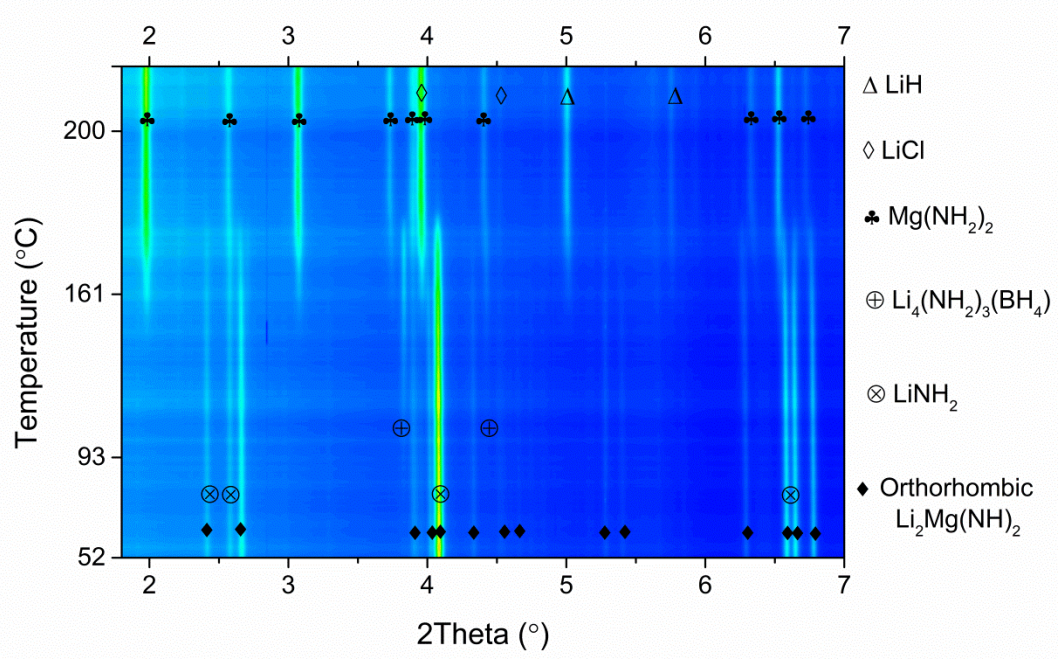

Figure 7. *In situ* SR-PXD experiment during the re-hydrogenation of the co-doped system. The sample was heated from RT to 200 °C with a heating rate of 5 °C/min and kept at 200 °C for 10 min under 85 bar of H_2.

The re-hydrogenation process was also measured by using *in situ* SR-PXD (**Figure 7**). The Bragg reflections of $Mg(NH_2)_2$ start to appear already at about 150 °C. However, it can be noticed that at ca. 170 °C they suddenly increased in intensity, indicating that the reaction proceeded very fast at this temperature, which correlates with the result of Figure 4. For this reason, the temperature of 170 °C was chosen for the cycling tests. At 200 °C, the absorption process is completed: the formation of $Mg(NH_2)_2$, LiH and LiCl (Figure 7), is in agreement with the PXD data of the starting material (Figure 6). The presence of $Li_4(NH_2)_3(BH_4)$ is also observed during the absorption process, until the temperature reached its melting point. Therefore $Li_4(NH_2)_3(BH_4)$ is involved in both the desorption and absorption processes.

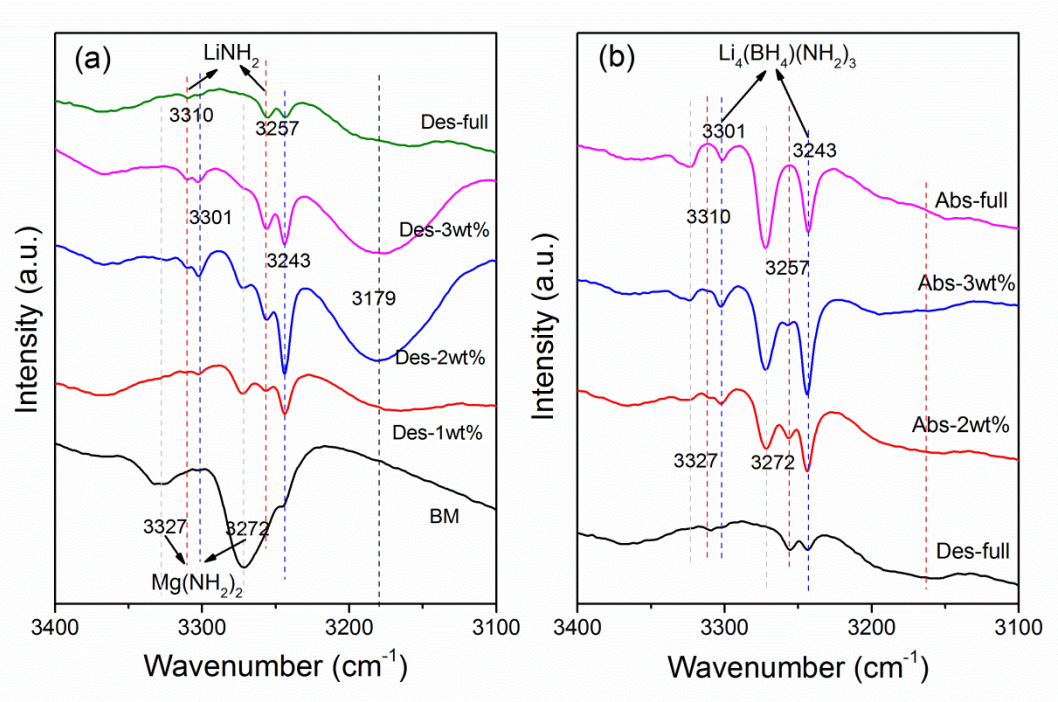

Figure 8. FTIR spectra of the co-doped sample at different stages of the (a) dehydrogenation (Des) and (b) absorption (Abs) processes.

Due to the limitations of XRD technique for the identification of amorphous and nano-crystalline phases, samples at different de/re-hydrogenation stages were investigated *via* FTIR technique (**Figure 8**). The FTIR spectrum of the sample after ball milling (Figure 8a) shows the N-H

stretching peaks belonging to $Mg(NH_2)_2$ (3327/3272 cm^{-1}) and $Li_4(NH_2)_3(BH_4)$ (3301/3243 cm^{-1}), which matches well with the phases observed in the *in situ* SR-PXD experiment (Figure 6). This result confirms that Li_3N indeed reacts with $LiBH_4$ to produce amorphous $Li_4(NH_2)_3(BH_4)$, and the *in situ* formed $Li_4(NH_2)_3(BH_4)$ may stabilize the crystalline structure of $Mg(NH_2)_2$, herein, improving the dehydrogenation kinetics (Figure 3). The new N-H stretching signals at 3310, 3257 and 3179 cm^{-1} are present in all the intermediate stages of dehydrogenation as well as in the fully dehydrogenated sample indicating that $LiNH_2$ and $Li_2Mg(NH)_2$ appeared together during the dehydrogenation process. The presence of $LiNH_2$ in this mixture is due to the hydrogenation of Li_3N. Figure 8(b) indicates that increasing the extent of hydrogenation, $LiNH_2$ and $Li_2Mg(NH)_2$ gradually convert to $Mg(NH_2)_2$. Surprisingly, the peaks corresponding to $Li_4(NH_2)_3(BH_4)$ continuously exists during the whole desorption/absorption cycle, independently from the formation of $LiNH_2$, which agrees well with the information obtained from *in situ* SR-PXD. The combination of FT-IR and *in situ* SR-PXD techniques confirmed that Li_3N might play an important role to assist the formation of $Li_4(NH_2)_3(BH_4)$, which at this point appears to be responsible for the weaker N-H bonds,[27] faster transport of Li^+ and creation of a "liquid-like" reaction interface.[26, 28]

Regarding the role of YCl_3 in the de/re-hydrogenation process it was possible to obtain only partial information from the interpretation of *in situ* SR-PXD and FTIR results. In order to analyze the chemical states of Y in this system, samples at different de/re-hydrogenation stages were investigated by using EXAFS (**Figure 9**). The extracted EXAFS region of these samples and references were Fourier-transformed to display the radial distribution function (RDF) of the atoms around the resonant Y atoms. By comparing the RDFs of the samples and references, YMg_2 reference spectrum exhibits the highest similarity with the half desorbed, fully desorbed

and half absorbed samples; the BM and fully absorbed samples show broad peaks that could be due to the overlapping signals of YH_x (YH_2 or YH_3) and YMg_2.

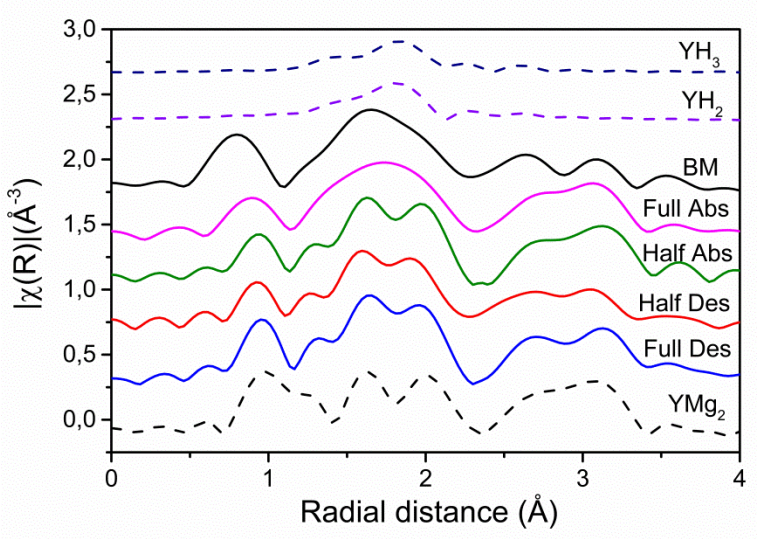

Figure 9. Radial distribution functions (Fourier transform of EXAFS spectra) of the co-doped sample at different hydrogenation stages: after ball milling (BM), half desorption (Half Des), full desorption (Full Des), half absorption (Half Abs), and full absorption (Full Abs).

YMg_2, most probably formed after ball milling, appears to be stable during the whole reaction. In principle, the *in situ* formed YH_x should react with LiB_4 to produce YB_x upon heating. Indeed YB_x compounds have been regarded as the active species[29] for improving the hydrogenation properties of borohydrides based systems doped with Y-salts. However, no information can be found for YB_x in the EXAFS measurements, this could be due to the low amount of YB_x or to a different reaction mechanism as compared to the $LiBH_4$-YH_3 system. In addition, the exact amount of hydrogen atoms of the YH_x phases cannot be determined based on the data reported in Figure 9, owing to the similar radial distributions of YH_2 and YH_3 and low X-ray scattering factors of hydrogen atoms. To clarify these aspects, the same samples were further characterized by combination of HR-TEM and energy dispersive X-ray spectroscopy (EDS). The results of these analyses are summarized in **Figure 10** (more detailed information is presented in **Figure**

S5). The EDS analysis shows the presence of YH_3 and YMg_2 in the ball milled sample, and the HR-TEM images indicated that the sizes of YH_3 and YMg_2 crystallites are ca. 2-5 and 10 nm, respectively. YB_4, YB_{12} along with YMg_2 are visible in the half dehydrogenated, fully dehydrogenated and half re-hydrogenated samples, while YH_3 is missing in these states. In the fully re-hydrogenated sample, YH_3 is visible again together with the disappearance of YB_4 and YB_{12}, this indicates that during the reversibility the chemical states of Y are cycling between YH_3 and YB_x (x=4 and 12). Similarly to the EXAFS results (Figure 9), the YMg_2 is present also in all the investigated samples (**Figure S6**). The chemical states and particle sizes analyses of YB_4 and YB_{12} species are shown in **Figure S7**. The detailed information about the chemical states of Y species and their related particle sizes are summarized in Table 2. All the YH_3 and YB_x species are nanostructured in the size range of 2-10 nm. These results also clarify why YH_3, YB_4 and YB_{12} could not be detected in the *in situ* SR-PXD analyses.

Table 2. Summary of the nanostructured particles and average sizes of the crystalline domains.

Samples	Found phases	Sizes
After Milling	YH_3 and YMg_2	YH_3 ~ 2 – 5 nm / YMg_2 ~ 10 nm
After half Hydrogenation	YB_4, YB_{12} and YMg_2	YB_x ~ 3-5 nm (x = 4 and 12) / YMg_2 ~ 10 nm
After full Hydrogenation	YH_3 and YMg_2	YH_3 ~ 10 nm / YMg_2 ~ 10 nm
After full Dehydrogenation	YB_4, YB_{12} and YMg_2	YB_x ~ 3 – 5 nm (x = 4 and 12) / YMg_2 ~ 10 nm
After half Dehydrogenation	YB_4, YB_{12} and YMg_2	YB_x ~ 3 – 5 nm (x = 4 and 12) / YMg_2 ~ 10 nm

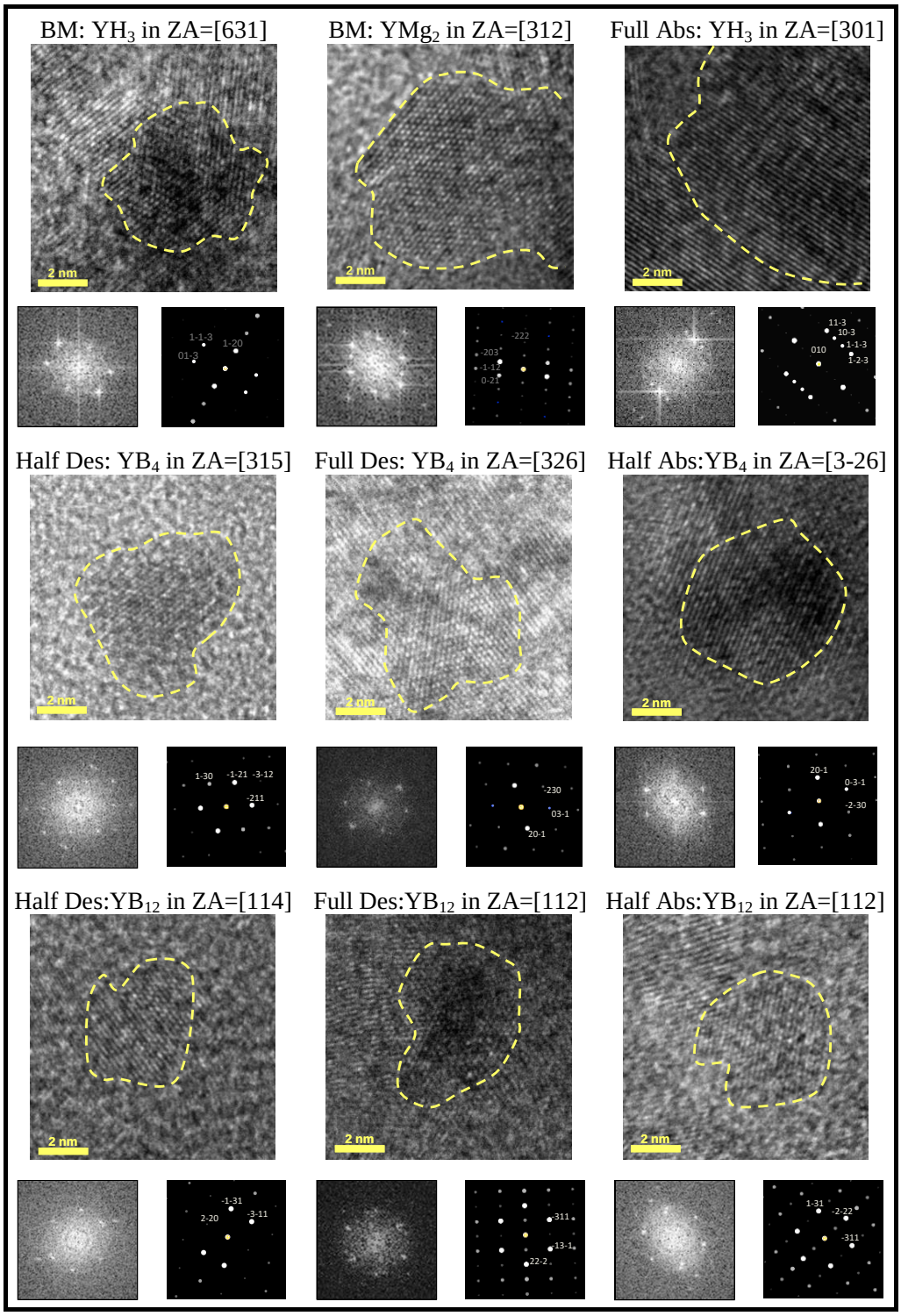

Figure 10. HR-TEM images of nanostructured Y-based compounds in each of the analyzed absorption/desorption stages. The calculated FFT from every particle is matched to a simulated zone axis (ZA) diffraction pattern to identify the corresponding phases and orientations. Every HR image in this Figure is 10 nm wide, while every FFT/DP has 18.5 nm^{-1} width.

A depicted representation of reason laying behind the excellent re-hydrogenation properties of the co-doped sample are shown in Scheme 1. During the re-hydrogenation process, H_2 is dissociated with the assistance of $YB_{x,}$ and then YB_x reacts with H_2 to produce YH_3. Differently from the direct hydrogenation of $Li_2Mg(NH)_2$ (which occurs in solid state), the hydrogen dissociated on the surface of YB_x/YH_3 can then further react with $Li_2Mg(NH)_2$ forming $Mg(NH_2)_2$ and LiH. Moreover, the presence of liquid $Li_4(NH_2)_3(BH_4)$ is likely to enhance the mass transfer between the reaction partners.

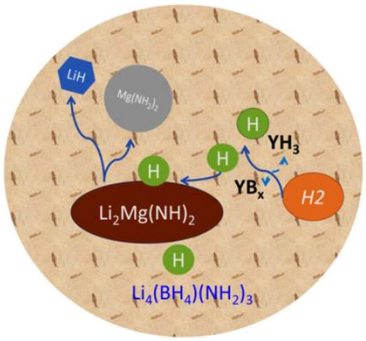

Scheme 1. The proposed absorption reaction mechanism of the co-doped sample.

Conclusions

The co-doping effects of Li_3N and YCl_3 on the $6Mg(NH_2)_2$-9LiH-$LiBH_4$ system were investigated systematically. The co-doped sample showed increased hydrogen capacity as well as faster de/re-hydrogenation kinetics, especially during the absorption process. About 4.2 wt % of H_2 can be charged within 8 min at 180 °C and 85 bar H_2. Increasing H_2 pressure above 185 bar, the re-hydrogenated temperature for fully charging the material can be reduced to 90 °C. Noticeably, this temperature falls within the operating temperatures range of PEMFCs. Our results show that the use of Li_3N and YCl_3 as co-additives improves the de/re-hydrogenation properties of the composite not only for the first dehydrogenation, but also over several de/re-

hydrogenation cycles. The experimental evidences were collected by means of volumetric technique, *in situ* SR-PXD, FTIR, EXAFS and HR-TEM, it is reasonable to conclude that: 1) the *in situ* formed $Li_4(NH_2)_3(BH_4)$, an excellent ionic conductor, improves the Li^+ transport while in solid state and in liquid state provides a fast means of transportation for the reacting species (e.g. $LiNH_2$ and $LiBH_4$). 2) The YB_x nanostructured particles assist the dissociation of H_2 reducing the energy required for breaking the H-H bond. In addition, the activation energies calculated for the dehydrogenation process also indicated that the co-doped system has the lowest E_a as compared with the systems containing only single dopants. Furthermore, the times required for a full re-hydrogenation process were reduced to 8 min and the absorption temperatures to 90 °C, making this co-doped system a promising on-board hydrogen storage material.

Experimental Details

$Mg(NH_2)_2$ (> 95%), supplied by Ping Chen's group, was synthesized by reaction of metallic Mg with ammonia at 300 °C. LiH and YCl_3 were purchased from Alfa-Aesar with a purity of 97% and 99.9%, respectively. $LiBH_4$ (95%) and Li_3N (99.5%) were bought from Sigma-Aldrich. All the samples were mixed according to their ratios and then ball milled 36 h at 200 rpm using a Fritsch Pulverisette 6 classic line planetary mill, with a ball to powder ratio of ca. 40:1. All powders handling and milling were performed in an MBraun argon glovebox with H_2O and O_2 levels below 10 ppm to prevent contamination.

Differential thermal analyses (DTA) as well as mass spectrometry (TPD-MS) measurements were carried out using a Netzsch STA 409 C and a Hiden Analytical HAL 201 Mass-Spectrometer combined system, with 50 mL min^{-1} argon flow. The samples were measured in the temperatures range of 30-300 °C with a heating rate of 3 °C min^{-1}. De/re-hydrogenation measurements were performed using a Sieverts-type apparatus (Hera, Quebec, Canada). The

material was in isothermal conditions at 100, 140 and 180 °C under 50 bar of hydrogen; in addition, 50, 185 and 245 bar of H_2 were used for isothermal hydrogenation at 90 °C, respectively. The reversibility was investigated using a Hy-energy PCT pro 2000 isothermally at 170 °C under hydrogen pressure of 1 bar for desorption and 85 bar for absorption, respectively.

In situ synchrotron radiation powder X-ray radiation diffraction (SR-PXD) experiments were performed at the diffraction beamline P.02.1 in the PETRA III storage ring of the synchrotron facility "Desy", in Germany. The fixed wavelength (λ) was 0.20745 Å and patterns were acquired with a plate image detector (2048*2048 pixel, each of size 200*200 μm^2); with the distance from sample to detector was ca. 1400 mm. The powder was introduced into a quartz capillary tube and then fixed on a in house developed *in situ* cell,[30] which is able to control heating temperatures and operating pressures.[31] Dehydrogenation was conducted from room temperature (RT) to 300 °C, with a heating rate of 10 °C min^{-1} under vacuum. Hydrogenation was recorded from RT to 250 °C under 80 bar of H_2 with a heating ramp of 10 °C min^{-1}. The 2D image was integrated by FIT2D software.[32] Quantitative analyses were performed using MAUD software implementing the Rietveld approach.[33]

FT-IR measurements were conducted on a Bruker, Model Tensor 27. The sample was ground with anhydrous KBr which had been heated at 110 °C overnight before using it. The weight ratio of sample to KBr is about 30:1. Grounded samples were pressed at 3 tons for 2 min. The spectra were recorded in the range of 400-4000 cm^{-1} at RT with 32 times scans and a resolution of 4 cm^{-1}.

High resolution transmission electron microscopy (HR-TEM) images were obtained on a Tecnai G^2 microscope with an information limit of 0.12 nm and Schottky Emission gun operating at 200 kV. The 5wt%Li_3N-2wt%YCl_3-codoped materials were observed at

different conditions: after ball milling, half and full hydrogenation and half and full dehydrogenation. It is important to mention that for each condition more than 10 high resolution images were taken an analysed in order to assure the nanocrystalline structure and morphology of the yttrium (Y) containing phases. The samples for TEM were prepared by dispersing a small amount of powder on a commercial carbon coated copper grid inside a glove box and then directly introducing the specimen into the microscope. The samples were exposed to air for a very short time. In order to identify the Yttrium-rich zone, point elemental analyses via energy dispersive X-ray spectroscopy (EDS) were performed. TEM images processing have been done with the following programs: Digital Micrograph (License Nº 90294175), i-TEM (License Nº A2382500) and JEMs (License Nº IEb59yBDflUMh).

Extended X-ray absorption fine structure (EXAFS) spectra were measured at the K-edge of Y to investigate the structural changes of the Y-containing phases associated with de/re-hydrogenation processes. The EXAFS beamline at DORIS III (DESY, Germany) was used for the EXAFS measurements. The ideal amount of powders for measurements were calculated via the program XAFSMASS[34]. The samples were mixed with boron nitride (50 mg) in a mortar and pressed (5 bar) into pellets of ca. 10 mm in diameter. To keep oxygen and moisture away from the samples, the pellets were fixed in an aluminum sample holder plate and sealed with Kapton tape from both sides. All preparation and handling of specimens were carried out in a glove box with a purified argon atmosphere. The measurements were recorded in transmission mode at the K-edge of Y. EXAFS data processing and analyses have been performed using the IFEFFIT software package.[35]

Acknowledgements

This work was supported by the CAS-HZG collaborative project “RevHy”-“Study on the synthesis, structures and performances of complex hydrides systems for Reversible high capacity Hydrogen storage at low temperatures”. We appreciate the access to the beam line P02 at the PETRA III and DORIS III (DESY, Germany). We also thank the Helmholtz Energy Materials Characterization platform for equipment supporting which is financially supported by The Helmholtz Foundation. The research leading to these results has received funding from the European Marie Curie Actions under ECOSTORE grant agreement no. 607040.

Associated content

Supporting Information

The Supporting Information is available free of charge on the ACS Publications website at DOI: xxxxxxxx.

References

[1] H. Cao, G. Wu, Y. Zhang, Z. Xiong, J. Qiu, P. Chen, Journal of Materials Chemistry A 2014, 2, 15816.

[2] A. Hepbasli, Renewable & Sustainable Energy Reviews 2008, 12, 593; A. M. Omer, Renewable & Sustainable Energy Reviews 2008, 12, 2265.

[3] L. Schlapbach, A. Zuttel, Nature 2001, 414, 353.

[4] B. Bogdanovic, M. Schwickardi, Journal of Alloys and Compounds 1997, 253, 1; B. Bogdanovic, M. Felderhoff, S. Kaskel, A. Pommerin, K. Schlichte, F. Schuth, Advanced Materials 2003, 15, 1012; J. Chen, N. Kuriyama, Q. Xu, H. T. Takeshita, T. Sakai, Journal of Physical Chemistry B 2001, 105, 11214; J. Wang, A. D. Ebner, J. A. Ritter, Journal of the American Chemical Society 2006, 128, 5949; Z. T. Xiong, G. T. Wu, J. J. Hu, Y. F. Liu, P. Chen, W. F. Luo, J. Wang, Advanced Functional Materials 2007, 17, 1137.

[5] A. Zuttel, P. Wenger, S. Rentsch, P. Sudan, P. Mauron, C. Emmenegger, Journal of Power Sources 2003, 118, 1; H. W. Li, Y. G. Yan, S. Orimo, A. Zuttel, C. M. Jensen, Energies 2011, 4, 185; G. L. Soloveichik, Y. Gao, J. Rijssenbeek, M. Andrus, S. Kniajanski, R. C. Bowman, S. J. Hwan, J. C. Zhao, International Journal of Hydrogen Energy 2009, 34, 916; D. Ravnsbaek, Y. Filinchuk, Y. Cerenius, H. J. Jakobsen, F. Besenbacher, J. Skibsted, T. R. Jensen, Angewandte Chemie-International Edition 2009, 48, 6659; K. Chlopek, C. Frommen, A. Leon, O. Zabara, M. Fichtner, Journal of Materials Chemistry 2007, 17, 3496; M. Paskevicius, L. H. Jepsen, P. Schouwink, R. Cerny, D. B. Ravnsbaek, Y. Filinchuk, M. Dornheim, F. Besenbacher, T. R. Jensen, Chemical Society Reviews 2017, 46, 1565; R. Gosalawit-Utke, T. K. Nielsen, I. Saldan, D. Laipple, Y. Cerenius, T. R. Jensen, T. Klassen, M. Dornheim, Journal of Physical Chemistry C 2011, 115, 10903; L. H. Rude, T. K. Nielsen, D. B. Ravnsbaek, U. Boesenberg, M. B. Ley, B. Richter, L. M. Arnbjerg, M. Dornheim, Y. Filinchuk, F. Besenbacher, T. R. Jensen, Physica Status Solidi a-Applications and Materials Science 2011, 208, 1754; C. B. Minella, C. Pistidda, S. Garroni, P. Nolis, M. D. Baro, O. Gutfleisch, T. Klassen, R. Bormann, M. Dornheim, Journal of Physical Chemistry C 2013, 117, 3846.

[6] P. Chen, Z. Xiong, J. Luo, J. Lin, K. L. Tan, Nature 2002, 420, 302.
[7] P. Chen, M. Zhu, Materials Today 2008, 11, 36; H. Cao, Y. Zhang, J. Wang, Z. Xiong, G. Wu, P. Chen, Progress in Natural Science: Materials International 2012, 22, 550; P. Chen, E. Akiba, S.-i. Orimo, A. Zuettel, L. Schlapbach, in *Hydrogen Science and Engineering : Materials, Processes, Systems and Technology*, Wiley-VCH Verlag GmbH & Co. KGaA, 2016, 763.
[8] S.-i. Orimo, Y. Nakamori, J. R. Eliseo, A. Züttel, C. M. Jensen, Chemical Reviews 2007, 107, 4111; J. Yang, A. Sudik, C. Wolverton, D. J. Siegel, Chemical Society Reviews 2010, 39, 656.
[9] H. Y. Leng, T. Ichikawa, S. Hino, N. Hanada, S. Isobe, H. Fujii, The Journal of Physical Chemistry B 2004, 108, 8763; Y. Nakamori, G. Kitahara, S. Orimo, Journal of Power Sources 2004, 138, 309; Y. Nakamori, G. Kitahara, K. Miwa, N. Ohba, T. Noritake, S. Towata, S. Orimo, Journal of Alloys and Compounds 2005, 404–406, 396.
[10] W. Luo, Journal of Alloys and Compounds 2004, 381, 284; Z. Xiong, G. Wu, J. Hu, P. Chen, Advanced Materials 2004, 16, 1522.
[11] Z. Xiong, J. Hu, G. Wu, P. Chen, W. Luo, K. Gross, J. Wang, Journal of Alloys and Compounds 2005, 398, 235; W. Luo, S. Sickafoose, Journal of Alloys and Compounds 2006, 407, 274.
[12] Y. Liu, K. Zhong, K. Luo, M. Gao, H. Pan, Q. Wang, Journal of the American Chemical Society 2009, 131, 1862; H. Cao, Y. Zhang, J. Wang, Z. Xiong, G. Wu, J. Qiu, P. Chen, Dalton Transactions 2013, 42, 5524; H. Cao, H. Wang, T. He, G. Wu, Z. Xiong, J. Qiu, P. Chen, Rsc Advances 2014, 4, 32555.
[13] P. Chen, Z. Xiong, J. Luo, J. Lin, K. L. Tan, The Journal of Physical Chemistry B 2003, 107, 10967; P. Chen, Z. Xiong, L. Yang, G. Wu, W. Luo, The Journal of Physical Chemistry B 2006, 110, 14221; E. Weidner, F. Dolci, J. Hu, W. Lohstroh, T. Hansen, D. J. Bull, M. Fichtner, The Journal of Physical Chemistry C 2009, 113, 15772; H. Wu, Journal of the American Chemical Society 2008, 130, 6515.
[14] J. Wang, T. Liu, G. Wu, W. Li, Y. Liu, C. M. Araújo, R. H. Scheicher, A. Blomqvist, R. Ahuja, Z. Xiong, P. Yang, M. Gao, H. Pan, P. Chen, Angewandte Chemie International Edition 2009, 48, 5828; W. Luo, V. Stavila, L. E. Klebanoff, International Journal of Hydrogen Energy 2012, 37, 6646; C. Liang, Y. Liu, M. Gao, H. Pan, Journal of Materials Chemistry A 2013, 1, 5031; Y. Liu, C. Li, B. Li, M. Gao, H. Pan, Journal of Physical Chemistry C 2013, 117, 866; T. Durojaiye, J. Hayes, A. Goudy, International Journal of Hydrogen Energy; T. Durojaiye, J. Hayes, A. Goudy, The Journal of Physical Chemistry C 2013, 117, 6554.
[15] H.-J. Lin, H.-W. Li, B. Paik, J. Wang, E. Akiba, Dalton Transactions 2016, 45, 15374; G. Xia, X. Chen, C. Zhou, C. Zhang, D. Li, Q. Gu, Z. Guo, H. Liu, Z. Liu, X. Yu, Journal of Materials Chemistry A 2015, 3, 12646; B. Li, S. S. Kaye, C. Riley, D. Greenberg, D. Galang, M. S. Bailey, ACS Combinatorial Science 2012, 14, 352.
[16] Q. Wang, Z. Chen, W. Yu, Y. Chen, Y. Li, Industrial & Engineering Chemistry Research 2010, 49, 5993; Q. Wang, Y. Chen, G. Niu, C. Wu, M. Tao, Industrial & Engineering Chemistry Research 2009, 48, 5250; S. Nayebossadri, International Journal of Hydrogen Energy 2011, 36, 8335; L.-P. Ma, H.-B. Dai, Z.-Z. Fang, X.-D. Kang, Y. Liang, P.-J. Wang, P. Wang, H.-M. Cheng, The Journal of Physical Chemistry C 2009, 113, 9944.
[17] J. Yang, A. Sudik, D. J. Siegel, D. Halliday, A. Drews, R. O. Carter, III, C. Wolverton, G. J. Lewis, J. W. A. Sachtler, J. J. Low, S. A. Faheem, D. A. Lesch, V. Ozolins, Angewandte Chemie-International Edition 2008, 47, 882; J. Yang, S. Hirano, Advanced Materials 2009, 21, 3023.
[18] J. Hu, M. Fichtner, P. Chen, Chemistry of Materials 2008, 20, 7089; H. Pan, S. Shi, Y. Liu, B. Li, Y. Yang, M. Gao, Dalton Transactions 2013, 42, 3802.
[19] J. Hu, Y. Liu, G. Wu, Z. Xiong, Y. S. Chua, P. Chen, Chemistry of Materials 2008, 20, 4398.
[20] L. M. Arnbjerg, D. B. Ravnsbæk, Y. Filinchuk, R. T. Vang, Y. Cerenius, F. Besenbacher, J.-E. Jørgensen, H. J. Jakobsen, T. R. Jensen, Chemistry of Materials 2009, 21, 5772.
[21] H. E. Kissinger, Analytical Chemistry 1957, 29, 1702.
[22] K. J. Laidler, Journal of Chemical Education 1984, 61, 494.

[23] https://energy.gov/sites/prod/files/2017/05/f34/fcto_myrdd_table_onboard_h2_storage_systems_doe_targets_ldv_1.pdf
[24] J. Hu, E. Weidner, M. Hoelzel, M. Fichtner, Dalton Transactions 2010, 39, 9100.
[25] D. J. Siegel, C. Wolverton, V. Ozoliņš, Physical Review B 2007, 75, 014101.
[26] A. Borgschulte, M. O. Jones, E. Callini, B. Probst, S. Kato, A. Zuttel, W. I. F. David, S.-i. Orimo, Energy & Environmental Science 2012, 5, 6823.
[27] H. Wu, W. Zhou, T. J. Udovic, J. J. Rush, T. Yildirim, Chemistry of Materials 2008, 20, 1245.
[28] M. Matsuo, A. Remhof, P. Martelli, R. Caputo, M. Ernst, Y. Miura, T. Sato, H. Oguchi, H. Maekawa, H. Takamura, A. Borgschulte, A. Züttel, S.-i. Orimo, Journal of the American Chemical Society 2009, 131, 16389.
[29] J. W. Kim, K.-B. Kim, J.-H. Shim, Y. W. Cho, K. H. Oh, Microscopy and Microanalysis 2014, 20, 1798; K.-B. Kim, J.-H. Shim, K. H. Oh, Y. W. Cho, The Journal of Physical Chemistry C 2013, 117, 8028; J.-H. Shim, Y.-S. Lee, J.-Y. Suh, W. Cho, S. S. Han, Y. W. Cho, Journal of Alloys and Compounds 2012, 510, L9.
[30] U. Boesenberg, C. Pistidda, M. Tolkiehn, N. Busch, I. Saldan, K. Suarez-Alcantara, A. Arendarska, T. Klassen, M. Dornheim, International Journal of Hydrogen Energy 2014, 39, 9899.
[31] C. Pistidda, A. Santoru, S. Garroni, N. Bergemann, A. Rzeszutek, C. Horstmann, D. Thomas, T. Klassen, M. Dornheim, The Journal of Physical Chemistry C 2015, 119, 934.
[32] A. Hammersley, European Synchrotron Radiation Facility Internal Report ESRF97HA02T 1997, 68.
[33] H. Rietveld, Acta Crystallographica 1967, 22, 151; H. Rietveld, Journal of applied Crystallography 1969, 2, 65.
[34] https://intranet.cells.es/Beamlines/CLAESS/software/xafsmass.html
[35] B. Ravel, M. Newville, Journal of synchrotron radiation 2005, 12, 537.

ToC

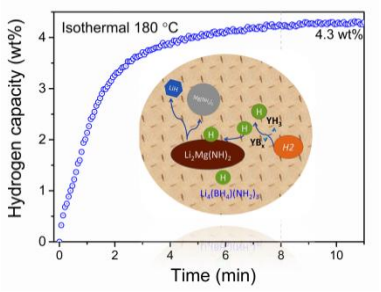

The synergetic effects of Li_3N and YCl_3 enable the $6Mg(NH_2)_2$-9LiH-$LiBH_4$ system to fully re-hydrogenate within 8 min.